Reversed deep-sea carbonate ion basin gradient during Paleocene-Eocene thermal maximum

Richard E. Zeebe[1] and James C. Zachos[2]

[1]   The Paleocene-Eocene thermal maximum (PETM, $\sim$55 Ma ago) was marked by widespread $CaCO_3$ dissolution in deep-sea sediments, a process that has been attributed to massive release of carbon into the ocean-atmosphere system. The pattern of carbonate dissolution is key to reconstructing changes in deep sea carbonate chemistry and, ultimately, the rate, magnitude, and location of carbon input. Here we show that during the PETM, the deep-sea undersaturation was not homogeneous among the different ocean basins. Application of a sediment model to a suite of data records from different sites and ocean basins shows that a globally uniform decrease in deep-sea carbonate ion concentration ($[CO_3^{2-}]$) is inconsistent with the data. Rather, we demonstrate that deep-sea $[CO_3^{2-}]$ increased from the Atlantic through the Southern Ocean into the Pacific. Our results show that the PETM deep-sea $[CO_3^{2-}]$ basin gradient during dissolution was reversed relative to the modern.

Citation: Zeebe, R. E., and J. C. Zachos (2007), Reversed deep-sea carbonate ion basin gradient during Paleocene-Eocene thermal maximum, *Paleoceanography*, *22*, PA3201, doi:10.1029/2006PA001395.

1.   Introduction

[2]   Rapid global warming and substantial changes in carbon cycling followed the Paleocene-Eocene Boundary (PEB, about 55 Ma ago) as documented by oxygen and carbon isotope and other records [*Kennett and Stott*, 1991]. Surface temperatures rose globally by $5-9°C$ and the ratio of $^{13}C/^{12}C$ of the surficial carbon reservoirs dropped by $\sim$3‰ within a few thousand years [e.g., *Thomas et al.*, 2002; *Zachos et al.*, 2003; *Nunes and Norris*, 2006; *Bowen et al.*, 2006; *Sluijs et al.*, 2006]. One set of hypotheses attributes the event to massive release of oceanic methane, which caused ocean acidification (by subsequent oxidation of methane to CO_2) and greenhouse gas warming through atmospheric CH_4/CO_2 increases [*Dickens et al.*, 1995, 1997; *Svensen et al.*, 2004]. Other hypotheses implicate terrestrial or sedimentary carbon reservoirs as the primary source of carbon input [*Kurtz et al.*, 2003; *Higgins and Schrag*, 2006].

[3]   Regardless of source, massive carbon release should have lowered deep-sea carbonate ion concentration, triggering widespread dissolution of seafloor carbonate [*Broecker and Takahashi*, 1977; *Sundquist*, 1986; *Dickens et al.*, 1995]. Indeed, detailed %carbonate records document a global carbonate dissolution horizon at the P/E boundary [e.g., *Kennett and Stott*, 1991; *Thomas and Shackleton*, 1996; *Thomas et al.*, 1999; *Bralower et al.*, 1997, 2002] with the calcite compensation depth (CCD) shoaling by as much as 2 km in the Atlantic Ocean [*Zachos et al.*, 2005]. Carbon cycle and climate reorganizations of such magnitude pose a general challenge for our understanding and models of carbon cycling and climate. Specifically, in order to predict long-term consequences of the current and future release of anthropogenic CO_2 [*Caldeira and Wickett*, 2003], carbon cycle models need to be calibrated on timescales $>10^2$ y. However, such model calibration is difficult because of the short duration of the observational database. In this regard, the PETM may serve as a valuable case study of the longer-term response to massive carbon release.

[4]   The first step needed to constrain the magnitude and location of carbon input during the PETM is to reconstruct the pattern of change in deep-sea chemistry, starting with $[CO_3^{2-}]$, which drove the dissolution of deep-sea carbonates [cf. *Dickens*, 2000]. In this paper, we investigate deep-sea sediment dissolution during the PETM as recorded in a variety of sediment records covering different ocean basins (section 2). We employ a sediment model (section 3) to simulate the observed changes in %$CaCO_3$ over time. We show that a global, uniform deep-sea carbonate ion concentration ($[CO_3^{2-}]$) during the dissolution event is inconsistent with the data (section 4). On the contrary, deep-sea $[CO_3^{2-}]$ appears to have increased from the Atlantic through the Southern Ocean into the Pacific (section 4.6). Our study shows that during the PETM, the deep-sea $[CO_3^{2-}]$ basin gradient was reversed relative to the modern.

2.   Data

[5]   Figure 1 displays the location of sediment cores examined in the present study (drilled by the Ocean Drilling Program, ODP). These sites have sediment cores with %carbonate data across the PETM. Locations in the Atlantic include Sites 999 and 1001 from the Caribbean [*Bralower et al.*, 1997; *Röhl and Abrams*, 2000] and Sites 1262, 1263, and 1266 from a depth transect at Walvis Ridge [*Zachos et al.*, 2005]. The PETM section of the Southern Ocean Site 690 from Maud Rise in the Weddell Sea has been the

---

[1]School of Ocean and Earth Science and Technology, Department of Oceanography, University of Hawaii at Manoa, Honolulu, Hawaii, USA.
[2]Earth and Planetary Sciences Department, University of California, Santa Cruz, California, USA.
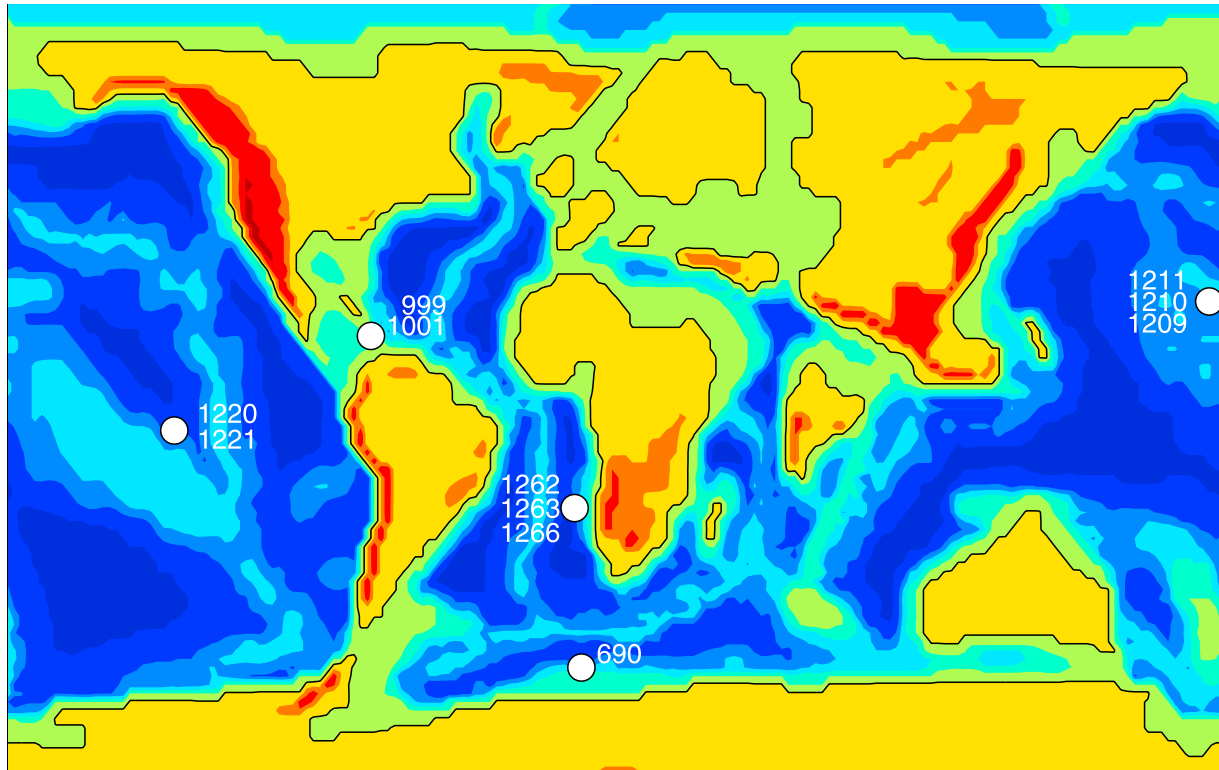
Figure 1. Data sites used in this study. Eocene topography from *Bice and Marotzke* [2002].

subject of several previous studies [e.g., *Kennett and Stott*, 1991; *Röhl et al.*, 2000; *Farley and Eltgroth*, 2003; *Kelly et al.*, 2005]. Locations in the Pacific include Sites 1220 and 1221 from the equatorial Pacific [*Lyle et al.*, 2002; *Murphy et al.*, 2006] and Sites 1209, 1210, and 1211 from a depth transect at Shatsky Rise [*Bralower et al.*, 2002; *Colosimo et*

al., 2005]. Further information on sediment cores are provided in Table 1 and section 4.

3. Sediment Model

[6] The sediment model calculates %$CaCO_3$ (dry weight) in the seafloor-bioturbated (mixed) sediment layer of thickness h_s as a function of sediment rain, dissolution, burial,

Table 1. $CaCO_3$ Records and Reconstructed Deep-Sea Saturation[a]

Site (Leg)	Location	Water Depth, m	Paleo Depth, m	Initial Sed. Rate, cm/ky	Initial $CaCO_3$, %	Reference	$[CO_3^{2-}]$ Min.,[b] μmol/kg	$[CO_3^{2-}]$ Min. (Ratio)
1266C (208)	Walvis Rdg. (S Atl)	3798	2600[c]	1.0	83	*Zachos et al.* [2005]	37	1
999 (165)	Caribbean (Atl)	2828	1500–2500[d]	3.20	60	*Röhl and Abrams* [2000]; *Bralower et al.* [1997]	<37	<1
1001 (165)	Caribbean (Atl)	3259	2000–2500[d]	3.80	67	*Röhl and Abrams* [2000]; *Bralower et al.* [1997]	<37	<1
690 (113)	Maud Rise (SO)	2914	2100[e]	1.5	85	*Kennett and Stott* [1991]; *Röhl et al.* [2000]; *Farley and Eltgroth* [2003]; *Kelly et al.* [2005]	48	1.30
1209B (198)	Shatsky Rise (N Pac)	2387	2400[f]	0.4	96	*Bralower et al.* [2002]; *Colosimo et al.* [2005]	52	1.41
1210B (198)	Shatsky Rise (N Pac)	2573	2600[f]	0.4	96	*Bralower et al.* [2002]; *Colosimo et al.* [2005]	54	1.46
1211C (198)	Shatsky Rise (N Pac)	2907	2900[f]	0.2	92	*Bralower et al.* [2002]; *Colosimo et al.* [2005]	58	1.57
1220B (199)	Central Trop. Pac	5218	2900[g]	1.1[h]	80	*Lyle et al.* [2002]; *Nunes and Norris* [2006]	49[i]	1.32
1221C (199)	Central Trop. Pac	5175	3300[g]	0.75[h]	50	*Murphy et al.* [2006]; *Nunes and Norris* [2006]	50[i]	1.35

[a]For further information on paleowater depth, see footnotes c, d, e, f, g and sections 4.1–4.5.
[b]Minimum deep $[CO_3^{2-}]$ during simulated dissolution (see Figure 5). Absolute values may be subject to revision (see text).
[c]*Zachos et al.* [2005].
[d]*Röhl and Abrams* [2000].
[e]*Kennett and Stott* [1991].
[f]*Bralower et al.* [2002].
[g]*Lyle et al.* [2002].
[h]Reported sedimentation rates apply to excursion rather than to initial values [*Nunes and Norris*, 2006].
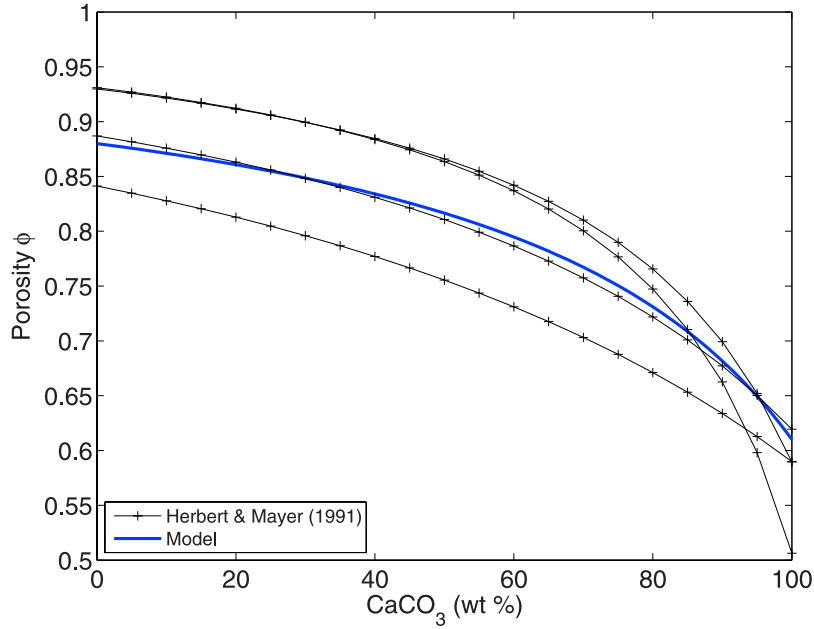[i]Initial model sedimentation rates were increased to fit observed %$CaCO_3$.

Figure 2. Relationship between porosity and %CaCO$_3$. Observations (+) after *Herbert and Mayer* [1991] (cf. their Table 1, hyperbolic fit). The solid thick line shows the non-linear relationship between ϕ and %CaCO$_3$ for a sediment layer composed of CaCO$_3$, clay, and water used in the model (equation (3)).

and chemical erosion. Equations are given in Appendix A. The model, which is particularly useful for long-term integrations, is similar to other models of this class [*Keir*, 1982; *Sundquist*, 1986; *Sigman et al.*, 1998]. However, the current model also includes variable porosity, a feature critical to simulating strong dissolution events that lead to sediment erosion, such as during the PETM.

3.1. Chemical Erosion

[7] When dissolution of CaCO$_3$ exceeds the rain of CaCO$_3$ plus clay, the sediment column shrinks and previously deposited, underlying sediment is reintroduced into the top layer and exposed to dissolution. This is referred to as chemical erosion. As a result, significantly more CaCO$_3$ is available for dissolution during erosion than originally contained in the top sediment layer. Once the top layer is entirely filled with clay, the sediment column is "sealed" and dissolution ceases.

[8] Many PETM deep-sea carbonate sections, including all those discussed in this study, display decreases in carbonate content. At certain locations, there are clay-rich layers (%CaCO$_3 \simeq 0\%$) of variable thickness, indicating that during peak dissolution, erosion did indeed occur (although not in uniform fashion). The model therefore needs to properly simulate this process. In order to fill the sediment top layer with clay, the sediment volume that was initially filled with CaCO$_3$+ pore water must be replaced by clay + pore water. Thus if the sediment porosity ϕ is constant, the ratio of total CaCO$_3$ available during erosion to the mass contained in the original surface layer is given by

$$1 + \frac{f_c^0}{(1 - f_c^0)} \tag{1}$$

[*Broecker and Takahashi*, 1977], where f_c^0 and $(1 - f_c^0)$ are the initial CaCO$_3$ and clay dry weight fraction of the sediment, respectively. However, if porosity varies with %CaCO$_3$ (as observations show, see below), the ratio of total dissolved to initial CaCO$_3$ is given by

$$1 + \frac{1 - \phi_0}{1 - \phi_1} \, \frac{f_c^0}{1 - f_c^0} \tag{2}$$

where ϕ_0 and ϕ_1 are the porosities of a pure clay and calcite layer, respectively. The factor $(1 - \phi_0)/(1 - \phi_1)$ is of the order $0.3-0.5$ and therefore significant as it reduces the erodible CaCO$_3$ from below the bioturbated layer by $50-70\%$ compared to the constant ϕ estimate [cf. *Archer*, 1996].

3.2. Variable Porosity

[9] In many locations it has been observed that porosity decreases with greater CaCO$_3$ fraction f_c [e.g., *Mayer*, 1991; *Herbert and Mayer*, 1991; *deMenocal et al.*, 1993]. That is, sediment with high CaCO$_3$ content has a higher concentration of total solids per unit volume than low carbonate sediment (Figure 2). The relationship between ϕ and f_c for a sediment layer composed of CaCO$_3$, clay, and pore water is given by

$$\phi = \frac{\phi_0 + f_c \, F}{1 + f_c \, F} \tag{3}$$

where $F = (\phi_1 - \phi_0)/(1 - \phi_1)$. Figure 2 shows equation (3) using $\phi_0 = 0.88$ and $\phi_1 = 0.61$ which falls within the range of data provided by *Herbert and Mayer* [1991] (cf. their Table 1, hyperbolic fit). The sediment model is based on
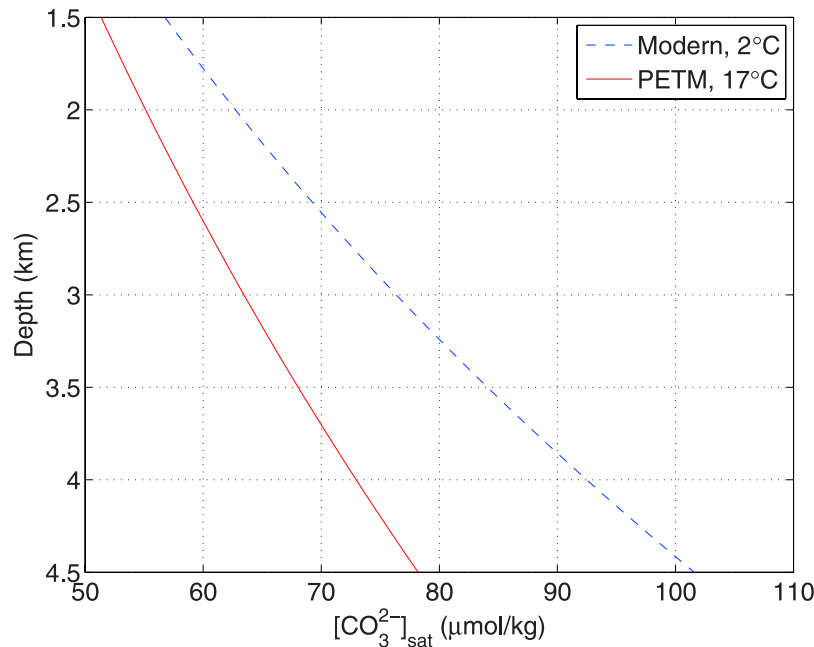
Figure 3. Calcite saturation concentration as a function of depth in the modern ocean and during Paleocene-Eocene thermal maximum (PETM) at deep ocean temperatures of 2 and 17°C, respectively.

these values for ϕ_0 and ϕ_1 and variable porosity given by equation (3). Note that using the nonlinear equation (3) in the model leads to the correct ratio of initial to erodible $CaCO_3$ (cf. equation (2), which was independently derived based on the geometry of the problem), while a linear relationship would not.

3.3. Calcite Saturation

[10] In the model, dissolution is calculated as a function of the difference between calcite saturation concentration ($[CO_3^{2-}]_{sat}$) and in situ carbonate ion concentration (see Appendix A). $[CO_3^{2-}]_{sat}$ is a function of temperature and pressure and varies mostly as a function of depth in the modern deep ocean (Figure 3). PETM deep ocean temperatures were higher, about 14–17°C [e.g., *Zachos et al.*, 2001; *Bice and Marotzke*, 2002; *Tripati and Elderfield*, 2005], which needs to be taken into account because of its effect on $[CO_3^{2-}]_{sat}$. The calcite saturation concentration during the PETM was calculated based on a deep ocean temperature of 17°C using temperature-dependent thermodynamic constants [*Mucci*, 1983; *Millero*, 1995; *Zeebe and Wolf-Gladrow*, 2001] available at www.soest.hawaii.edu/oceanography/faculty/zeebe.html. Figure 3 shows that the temperature effect is important for the PETM calcite saturation. First, deep-sea $[CO_3^{2-}]$ in equilibrium with calcite at 3.5 km depth would have been about 10 μmol kg^{-1} lower during PETM, compared to modern values. Second, PETM $[CO_3^{2-}]_{sat}$ is less sensitive to changes in depth.

[11] In addition to temperature, differences between modern and Eocene seawater composition (e.g., $[Ca^{2+}]$ and $[Mg^{2+}]$) would also affect $[CO_3^{2-}]_{sat}$. We tested the effect of doubling $[Ca^{2+}]$ and reducing $[Mg^{2+}]$ by 40% on calcite solubility using the approach described by *Tyrrell and Zeebe* [2004]. This

affected absolute values of deep-sea $[CO_3^{2-}]$ rather than its ratio, which is the focus of the present study (see section 4.6). We therefore report model deep-sea $[CO_3^{2-}]$ during the PETM at elevated temperature but at modern $[Ca^{2+}]$ and $[Mg^{2+}]$. We note that absolute numbers would change if adjusted to Eocene seawater composition.

4. Results

[12] In the following, the model is used to simulate the temporal evolution of sediment %$CaCO_3$ as provided by records introduced in section 2 (see Table 1). On the basis of the results of the Leg 208 depth transect at Walvis Ridge [*Zachos et al.*, 2005], a reference dissolution forcing will be established for the model (dubbed "south Atlantic forcing" or SA forcing), which is capable of capturing the essential features of the Walvis Ridge observations. Given that forcing, we will address the question: Can the PETM %$CaCO_3$ records from across the globe be qualitatively reproduced using a uniform undersaturation forcing?

4.1. Reference Case: South Atlantic, Walvis Ridge

[13] Detailed %$CaCO_3$ records across the PETM have been constructed for sites that comprise a depth transect down Walvis Ridge in the south Atlantic [*Zachos et al.*, 2005]. Sedimentation rates/age models for these PETM intervals are based on correlation to the PETM record at Site 690 [*Röhl et al.*, 2000] using 11 carbon isotope tie points from −125 to +230 ky relative to the PEB [see *Zachos et al.*, 2005, Table S4]. Three of those records spanning the full depth range (Sites 1263, 1266, and 1262, paleowater depths ~1500, 2600, and 3600 m [*Zachos et al.*, 2005]) and corresponding model results for %$CaCO_3$
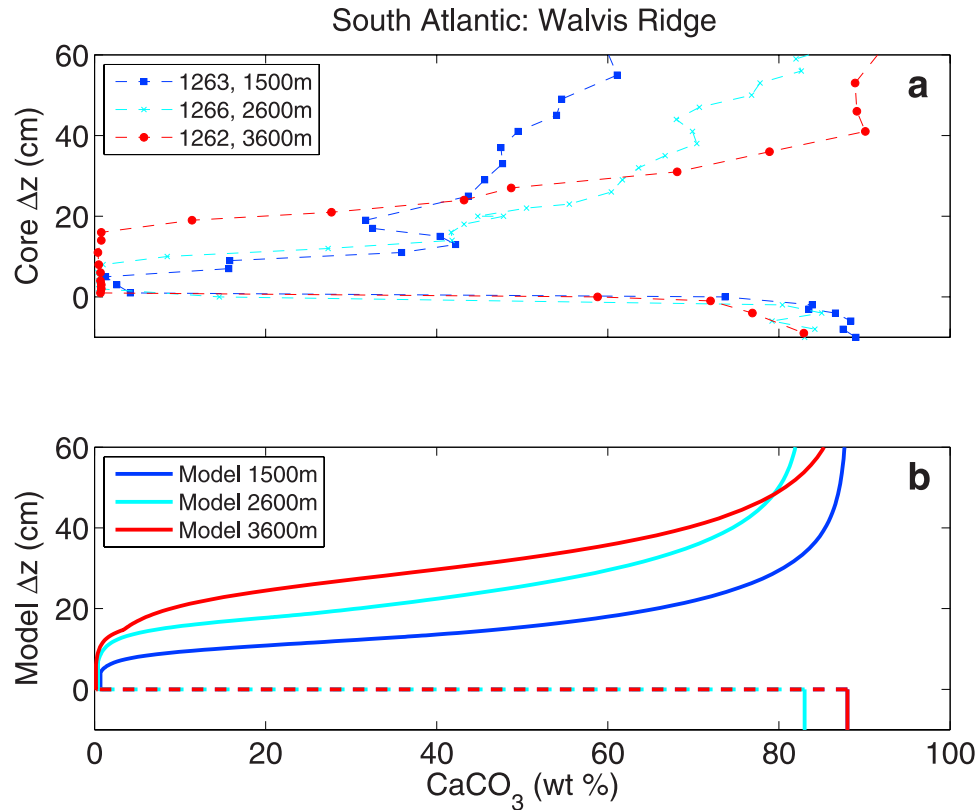
Figure 4. (a) Observed deep-sea %CaCO$_3$ sediment records during the PETM at Walvis Ridge [*Zachos et al.*, 2005]; paleowater depths as indicated. (b) Corresponding model results. Core and model Δz denote sediment depth above the Paleocene-Eocene boundary (PEB). All simulated records were generated with the exact same carbonate ion forcing (Figure 5), showing that the essential features of the Walvis Ridge records can be simulated using a uniform deep-sea [CO$_3{}^{2-}$] forcing. Note that the simulated erosion process, which leads to a descent of the sediment-water interface at the PEB, is not shown here. To facilitate comparison with observations, model curves during erosion have been replaced by horizontal dashed lines at the PEB in Figure 4b. See Figure 8c for erosion.

are shown in Figures 4a and 4b, respectively. The model results were obtained using the dissolution forcing (deep-sea [CO$_3^{2-}$] versus time) displayed in Figure 5. The minimum carbonate ion concentration during the first few tens of ky will be denoted by [CO$_3^{2-}$]$_{min}$. Note that absolute [CO$_3^{2-}$] values in units of μmol kg^{-1} discussed here should be viewed with caution because of differences in modern and Eocene seawater composition (see above) and potential differences in dissolution parameters (section 5.1). Fortunately, the main objective is to examine relative deep-sea saturation patterns between sites and ocean basins. This quantity as expressed by the relative carbonate ion concentration ratios in our results appears to be robust (section 4.6).

[14] A simple, linear forcing function (Figure 5) was deemed more appropriate for the primary goal of the simulations, which is to reproduce the significant features shared by all sediment records rather than the details of individual records. The significant features are (1) the minimum in %CaCO$_3$ during peak dissolution, (2) thickness of the minimum %CaCO$_3$ layer, and (3) timescale of return to initial values. For example, all simulated records in Figure 4b for 1500, 2600, and 3600 m were generated with

the exact same carbonate ion forcing. The differences in features 1–3 among the three graphs are thus only a result of the difference in initial %CaCO$_3$, sedimentation rate and water depth/[CO$_3^{2-}$]$_{sat}$ (all given by the data), and not of prescribed deep-sea [CO$_3^{2-}$] versus time. The bottom line of the model-data comparison for the reference case is that the essential features of the Walvis Ridge records can be broadly simulated using a uniform deep-sea [CO$_3^{2-}$] forcing.

4.2. Atlantic, Caribbean Plate

[15] Figure 6 shows corresponding data and model results for two Caribbean Sites 999 and 1001 [*Bralower et al.*, 1997; *Röhl and Abrams*, 2000]. The paleowater depth of Site 999, ~2000 m, is loosely based on benthic foraminifer assemblages, as is the depth of Site 1001 at ~2300 m [*Sigurdsson et al.*, 1997; *Röhl and Abrams*, 2000]. Regarding data resolution and age-model development, a brief comparison to the south Atlantic sites may be helpful. The published sedimentation rates for Sites 999 and 1001 are based on a correlation to Site 690 using two tie points at the base of the carbon isotope excursion (CIE) and the horizon where δ^{13}C stabilize [*Bralower et al.*, 1997]. Above and below, the
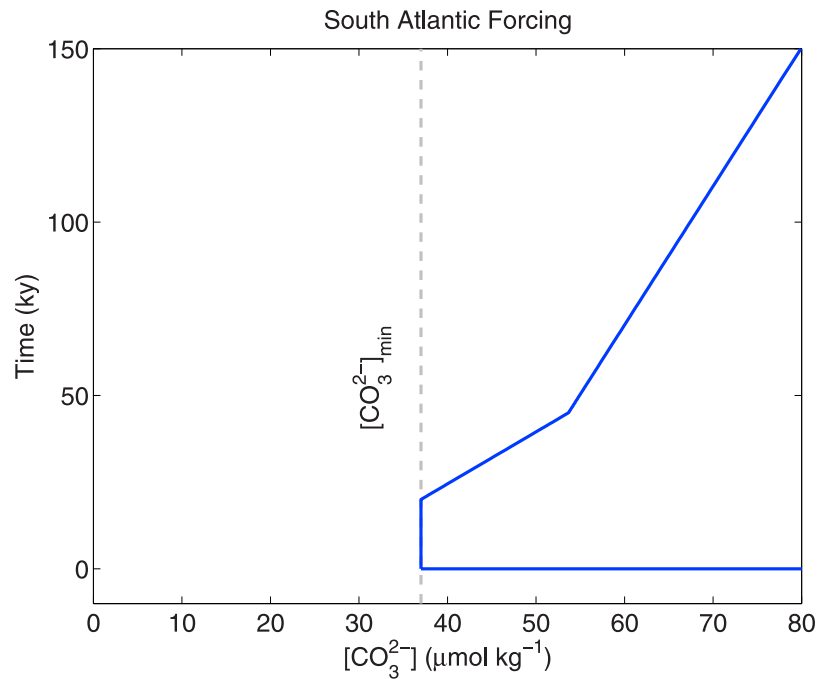
Figure 5. Reference $[CO_3^{2-}]$ model forcing as a function of time ("South Atlantic forcing" or SA forcing) used to simulate observations at Walvis Ridge (Figure 4). $[CO_3^{2-}]_{min}$ denotes the minimum carbonate ion concentration of the forcing. $[CO_3^{2-}]_{min}$ is modified for "adjusted forcing" scenarios (see text).
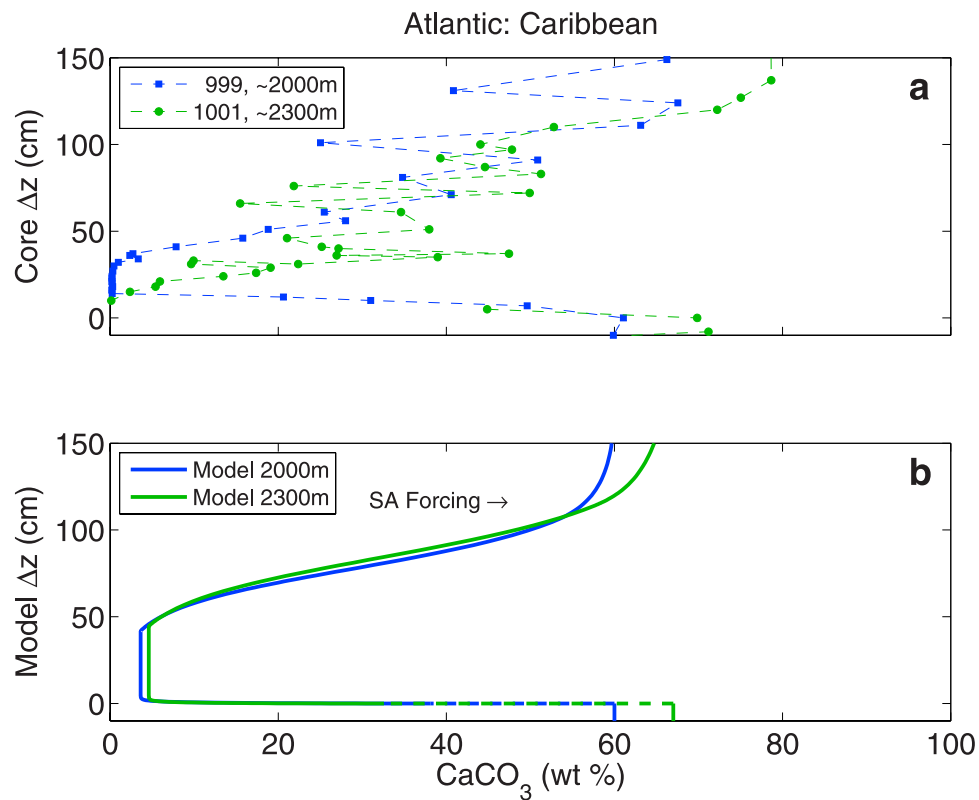

Figure 6. (a) Observed deep-sea %$CaCO_3$ sediment records during the PETM at two Caribbean sites [*Bralower et al.*, 1997]. (b) Model results using SA forcing as shown in Figure 5.
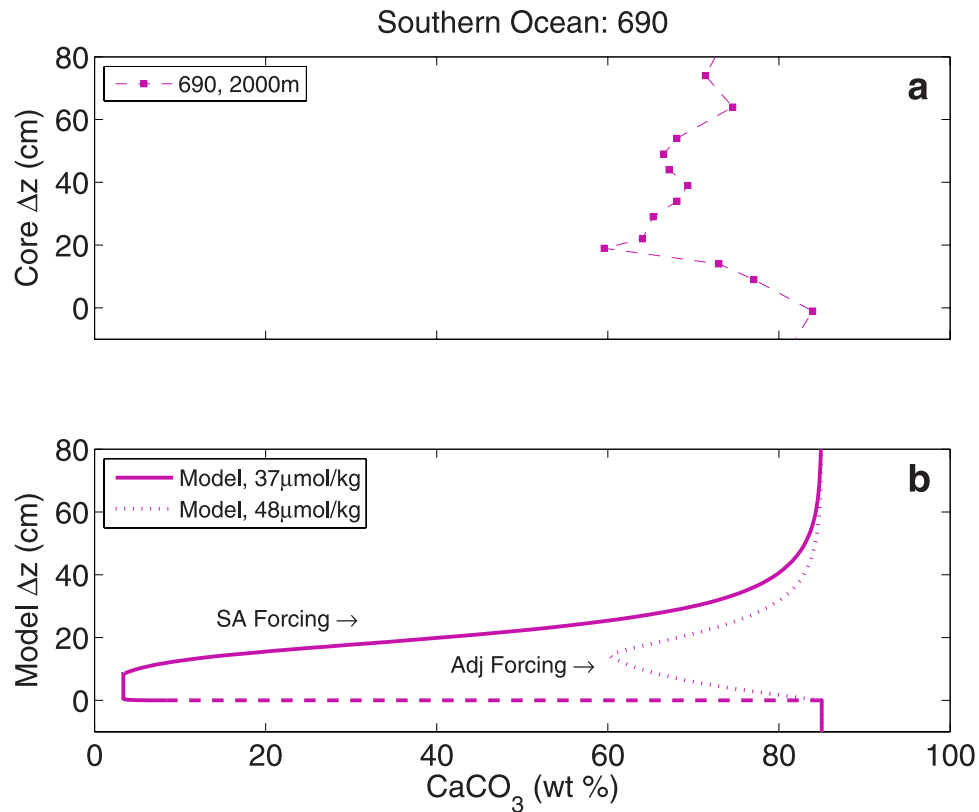
Figure 7. (a) Deep-sea %CaCO$_3$ data at Southern Ocean Site 690 during PETM [*Kelly et al.*, 2005]. (b) Model results using SA forcing as shown in Figure 5 (solid line) and adjusted forcing (dashed line, see text).

sedimentation rates are based on nannofossil datums at 56.2 and 55.3 Ma, corresponding to a sedimentation rate averaged over a window of almost 1 Ma that includes the entire PETM [*Sigurdsson et al.*, 1997]. Although pre-PETM sedimentation rates for the Caribbean sites are not as well constrained as the south Atlantic sites, it appears that the rates at 999 are significantly higher than at 1001 because of higher siliciclastic sediment flux. This explains an unusual observation; the paleowater depth of Site 1001 is greater than 999, yet the clay layer is substantially thinner. Moreover, both sites contain numerous ash layers which introduce random variability to sedimentation rates and carbonate content.

[16] Applying the south Atlantic forcing to these cores, we find that several features of initial model results do not match observations as well as for the Walvis Ridge. First, the modeled minimum %CaCO$_3$ layer is thicker than observed, particularly for Site 1001. Second, the simulated minimum %CaCO$_3$ values are higher than observed. In order to reconcile data and model, one would have to assume that the initial sedimentation rate was smaller than the reported average over ~1 Ma [*Sigurdsson et al.*, 1997; *Bralower et al.*, 1997]. In addition, a stronger prescribed undersaturation is required in the model to explain minimum %CaCO$_3$ values during peak dissolution.

[17] Despite these differences (which could potentially be reduced at higher data resolution for %CaCO$_3$ and sedimentation rates), the key observation is that the two Caribbean

sites at 1500–2500 m paleowater depth show strong dissolution and a sizeable clay layer during the PETM. The model predictions are broadly consistent with the observations when the SA forcing is applied, only that the model calls for stronger undersaturation. This is not the case for other ocean basins (see below).

4.3. Southern Ocean, Maud Rise

[18] Site 690 in the Southern Ocean (Maud Rise) has been extensively studied [e.g., *Kennett and Stott*, 1991; *Röhl et al.*, 2000; *Farley and Eltgroth*, 2003; *Kelly et al.*, 2005]. The paleowater depth of Site 690 during the P/E transition was 2100 m [*Kennett and Stott*, 1991]. The %CaCO$_3$ data and model results for this site are shown in Figure 7. In this case, application of the SA forcing yields a dissolution pattern that does not fit observation. Given the reported paleowater depth, sedimentation rate, and initial %CaCO$_3$ (Table 1), the model predicts low %CaCO$_3$ (<10%) during the peak dissolution phase using the SA deep-sea undersaturation of $[CO_3^{2-}]_{min} = 37$ μmol kg^{-1}, whereas the %CaCO$_3$ values drop from 85% to a minimum of only 60% at ~20 cm above the PEB. In order to match this pattern, the model requires less corrosive bottom water during peak dissolution (adjusted forcing, $[CO_3^{2-}]_{min} = 48$ μmol kg^{-1}). The relative ratio of Southern Ocean to south Atlantic deep-sea $[CO_3^{2-}]$ would thus be 48/37 = 1.30. For comparison, the modern ratio of, e.g., deep Pacific to deep
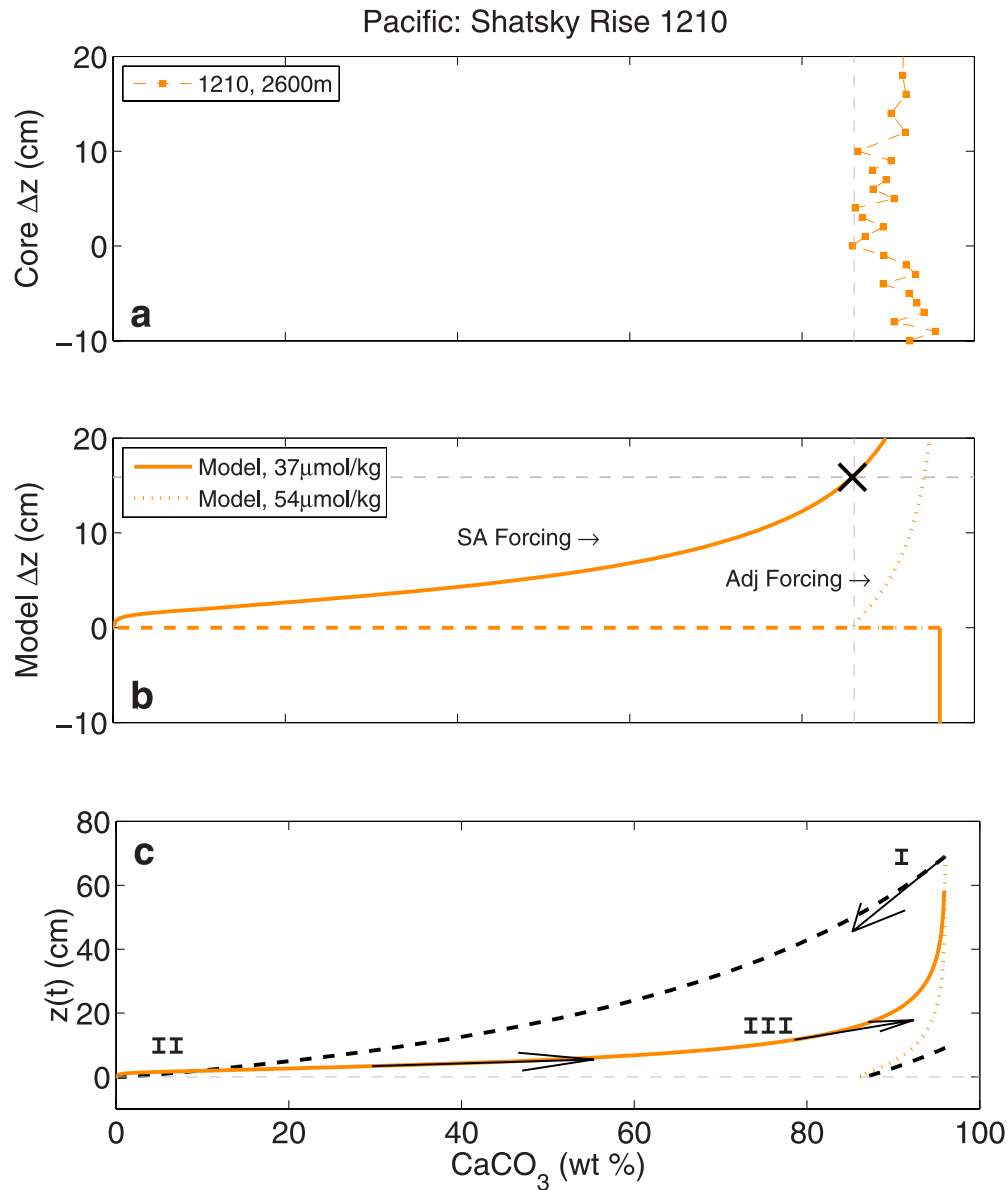
Figure 8. (a) PETM %CaCO$_3$ records at Shatsky Rise [*Colosimo et al.*, 2005]. (b) Model results using SA forcing as shown in Figure 5 (solid line) and adjusted forcing (dashed line, see text). (c) Erosion process across PEB (black dashed lines) as simulated by the model. Here $z(t)$ is the position of the sediment-water interface relative to the horizon where sediment accumulation resumes (Model $\Delta z = 0$). I: Onset of dissolution leads to erosion and descent of sediment-water interface down to II where erosion stops. III: Net accumulation has resumed. For the SA and adjusted forcing, erosion leads to a descent of the sediment-water interface by $\sim$70 cm and less than 10 cm, respectively.

Atlantic [CO$_3^{2-}$] at 3.5 km depth is about 70/100 = 0.7 [*Zeebe and Westbroek*, 2003]. For a discussion of the sensitivity of the calculated deep-sea [CO$_3^{2-}$] ratios during peak PETM dissolution with respect to model assumptions, see section 5.

[19] We note that the onset of the CIE at Site 690 is accompanied by a decline in carbonate content and coarse fraction as well as increased levels of shell fragmentation [*Kelly et al.*, 2005]. This suggests that the drop in %carbonate at 690 during the initial phase of the PETM was caused by

dissolution rather than a decrease in CaCO$_3$ production in the surface ocean [cf. *Bralower et al.*, 2004; *Stoll*, 2004].

4.4. Pacific, Shatsky Rise

[20] During Leg 198, a series of cores covering the PEB was obtained along a depth transect at Shatsky Rise [*Bralower et al.*, 2002; *Colosimo et al.*, 2005]. Water depths for Sites 1209–1212 range from 2387 m to 2907 m, similar to their estimated paleowater depth [*Bralower et al.*, 2002]. Figure 8 displays %CaCO$_3$ data and corresponding model results for the PETM

section at Site 1210. The observed %CaCO$_3$ record at this and all sites on Shatsky Rise exhibit less carbonate burn-down compared to the Atlantic sites. Even at the deepest Site 1211 ($\sim$3000 m paleowater depth), %CaCO$_3$ never drops below 70% during the PETM. However, we note that because samples were collected at 1 cm intervals, it is possible that carbonate content just at the contact is lower than shown in the records (XRF core scanning data shows a sharp peak in Fe content just at the contact, cf. also *Hancock and Dickens* [2005]).

[21] When comparing records at Shatsky Rise and Walvis Ridge, there are two important differences (Table 1, Figure 4). The sedimentation rates are generally lower and the carbonate contents are initially higher at Shatsky Rise. Note that a difference in initial %CaCO$_3$ of 96% versus 83% is substantial considering its effect on sediment erosion during peak dissolution. Equation (2) shows that the erosion depth is proportional to $f_c^0/(1 - f_c^0)$ which is 24.0 and 4.9 at $f_c^0 = 0.96$ and 0.83, respectively. In other words, if chemical erosion continues until the top layer is entirely filled with clay, a five to six times thicker sediment layer is removed at $f_c^0 = 0.96$ than at $f_c^0 = 0.83$ (erosion depth say 70 versus 12 cm depending on porosity, see below).

[22] As a result, given the larger initial %CaCO$_3$ of the Shatsky Rise sites plus lower sedimentation rates (which also means less clay rain per unit time), one could argue that a sizeable clay layer or a sizable %CaCO$_3$ drop may not have developed at Shatsky Rise, even if the deep Pacific and south Atlantic undersaturation was the same. Figure 8b shows that this is unlikely. Applying the SA forcing to initial conditions at Site 1210, the model does predict a clay layer (although thin, $\sim$1 cm). One may further argue that due to variations in the mixing depth, this may not be preserved in the actual sediment record. However, the SA forcing should generate $\sim$15 cm of sediment with %CaCO$_3$ significantly below 85% (cf. cross mark in Figure 8b). This is not recorded in the data. The observed %CaCO$_3$ at Site 1210 stays above $\sim$85% within the 20 cm above the PEB (base of excursion at $\Delta z = 0$).

[23] A scenario more consistent with the data would require a deep Pacific undersaturation of $[CO_3^{2-}]_{min} = 54$ μmol kg^{-1} during the peak dissolution phase (adjusted forcing). We conclude that despite higher initial %CaCO$_3$ and lower sedimentation rates, the Shatsky Rise records cannot be reproduced with the model using SA forcing. The model calls for less undersaturated bottom water. This conclusion holds for all Shatsky Rise sites (1209–1212). The required $[CO_3^{2-}]_{min}$ for Sites 1209–1211 (which includes the shallowest and deepest sites) are given in Table 1.

[24] Figure 8c illustrates the effect of initial %CaCO$_3$ on erosion depth as described above. The position of the sediment-water interface as a function of time is denoted by $z(t)$. Values of $z(t)$ are relative to the horizon where sediment accumulation resumes (model $\Delta z = 0$), corresponding to the time when sediment deposition and burial continue to generate the sediment record above the base of erosion. Using SA forcing and given $f_c^0 = 0.96$ at Site 1210, the sediment-water interface would descend by $\sim$70 cm before erosion ceases. For comparison, it is about 12 cm for Site 1266 in the south Atlantic (not shown). Thus there is a

significant difference during erosion whether initial %CaCO$_3$ is 96% or 83%. However, as explained above it is difficult to explain the lack of a sizeable %CaCO$_3$ decrease in the Shatsky Rise records with this mechanism. The evolution of $z(t)$ using adjusted forcing ($[CO_3^{2-}]_{min} = 54$ μmol kg^{-1}) is also shown in Figure 8c, in which case the interface descends by less than 10 cm.

[25] As for the validity of our assumption of constant carbonate flux across the boundary, we note that a rise in the production and vertical flux of calcareous plankton shells in the Pacific during the PETM could offset effects of increased dissolution on carbonate content, thus giving the appearance of less dissolution. However, the Shatsky Rise sites all show evidence of a reduction in plankton productivity during the PETM [*Kaiho et al.*, 2006].

4.5. Pacific, Mahi Mahi Fracture Zone

[26] Ocean Drilling Program Leg 199 recovered the PETM at sites in the Central Equatorial Pacific; %CaCO$_3$ data is available for Sites 1220 and 1221 [*Lyle et al.*, 2002; *Murphy et al.*, 2006]. Estimated paleowater depths of Sites 1220 and 1221 were 2900 and 3300 m during the Early Eocene [see *Lyle et al.*, 2002, Figure F12]. Sedimentation rates for these sites are based on a three-tie point correlation to Site 690 [*Nunes and Norris*, 2006] and actually apply to the excursion, rather than initial period (see Table 1). Preexcursion values, which are needed as model input, were possibly higher. Figure 9 shows data and model simulations for Site 1220. Using SA forcing, during peak dissolution the minimum %CaCO$_3$ drops close to $\sim$0% in the model, while the data bottom at 20%. Even a threefold higher sedimentation rate is insufficient to compensate (model minimum %CaCO$_3$ is still close to 0%). However, invoking a higher sedimentation rate together with a deep Pacific undersaturation of $[CO_3^{2-}]_{min} = 49$ μmol kg^{-1} during peak dissolution (adjusted forcing), yields a minimum %CaCO$_3$ that is close to the observed value of about 20%.

4.6. Carbonate Ion Basin-Gradient

[27] Figure 10 summarizes the deep-sea $[CO_3^{2-}]_{min}$ estimates that were obtained in the previous sections by adjusting the forcing in order to reproduce the dissolution features at the various sites. Because absolute values are subject to uncertainties (see above), we report $[CO_3^{2-}]_{min}$ ratios relative to the reference $[CO_3^{2-}]_{min}$ of the SA forcing. The color symbols indicate the model outcome using standard dissolution parameters (for other lines which indicate model sensitivity, see section 5.1). Our results show that deep-sea $[CO_3^{2-}]$ during the PETM dissolution period increased from the Caribbean toward the south Atlantic/Southern Ocean and reached the highest values in the deep Pacific. The deep $[CO_3^{2-}]$ basin gradient is therefore reversed compared to the modern pattern.

[28] We note that our $[CO_3^{2-}]$ reconstruction is based on the assumption that the %CaCO$_3$ differences between the various sites across the globe were caused by the bottom water CO_3^{2-} concentration. One could attempt to construct alternative causes based on say differences in surface production, bioturbation (section 5.2), rain ratio or alike. However, bottom water corrosiveness appears to be the first
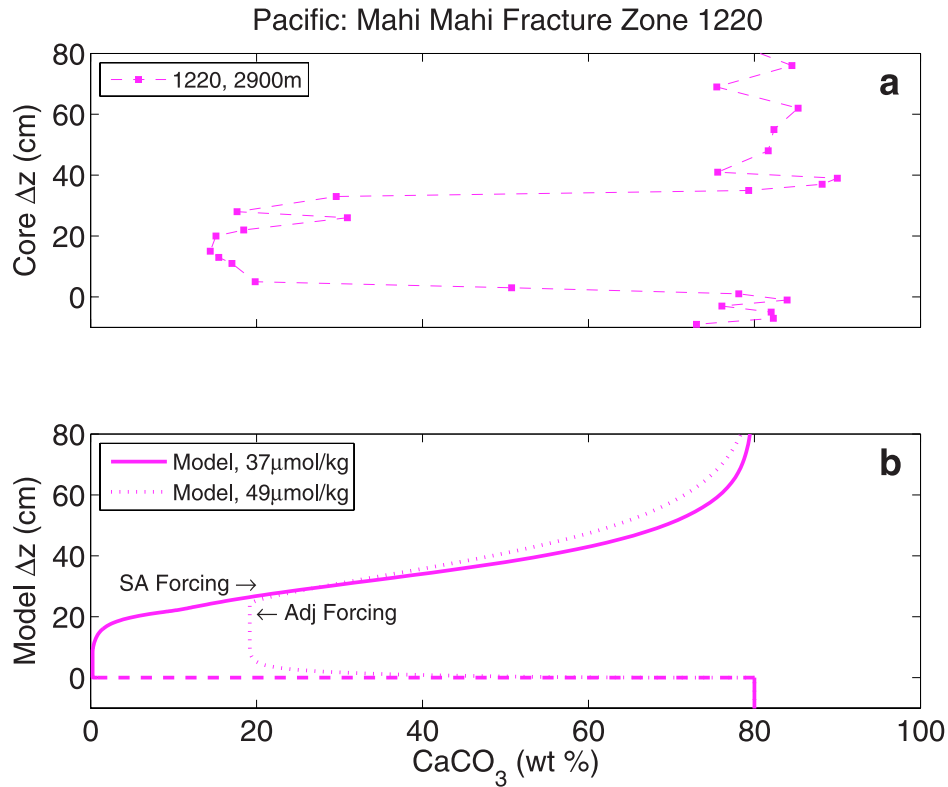
Figure 9. (a) Observed deep-sea %CaCO$_3$ during the PETM in the central tropical Pacific at 2900 m paleowater depth [*Lyle et al.*, 2002]. (b) Corresponding model results using SA and adjusted forcing (see text).
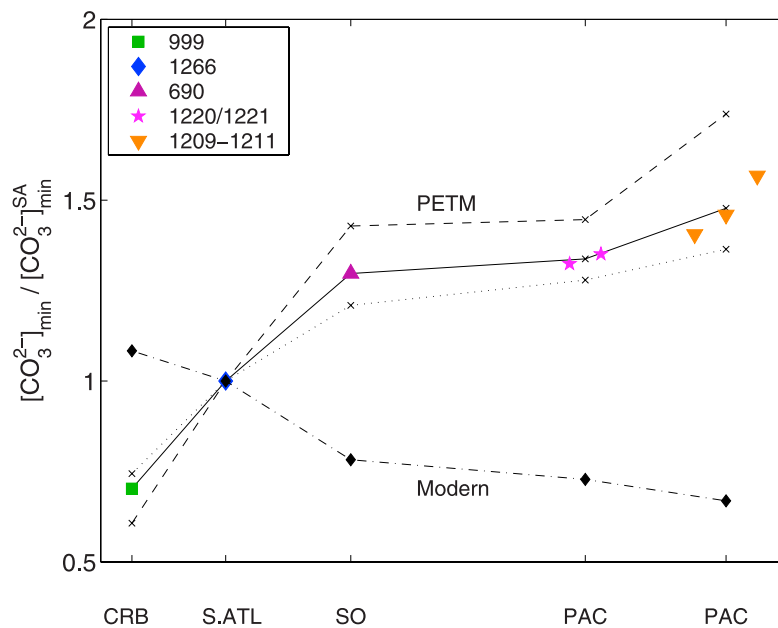

Figure 10. Reconstructed deep-sea [CO$_3^{2-}$] ion gradient between ocean basins during peak PETM dissolution phase. Shown are minimum [CO$_3^{2-}$] values as reconstructed for the various sites, relative to the minimum value of the SA forcing ([CO$_3^{2-}$]$_{min}^{SA}$, see Figure 5). CRB = Caribbean, S.ATL = south Atlantic, SO = Southern Ocean, PAC = Pacific. The solid line shows model results with standard model parameter; the dotted and dashed lines show results with stronger and weaker dissolution response in the model (see Figure 11). The modern gradient relative to the south Atlantic (dot-dashed line) was calculated using the GLODAP database [*Key et al.*, 2004].
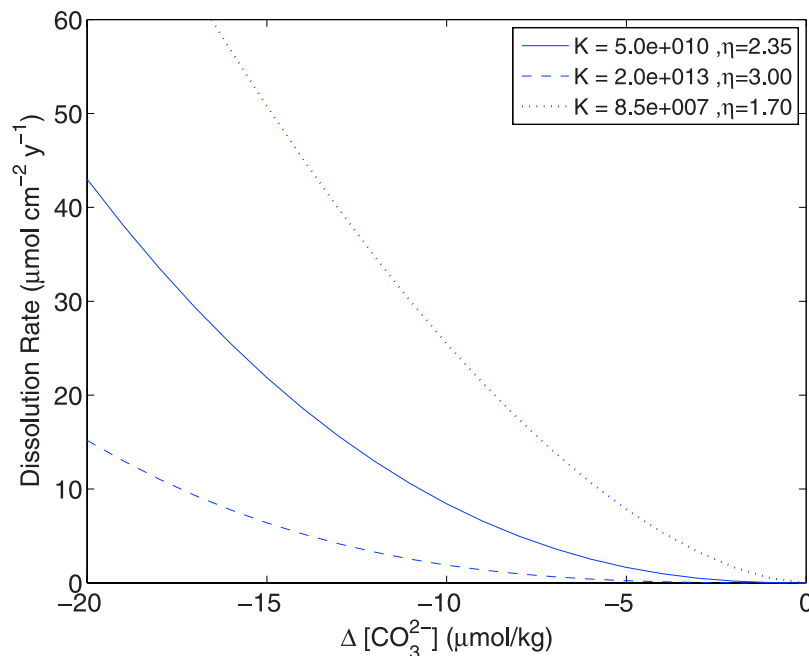
Figure 11. Variation of model dissolution parameters (cf. equation (A3)). The solid line indicates standard parameter (see legend for values; K in units of mol m^{-2} y^{-1}). Depending on the choice of parameter values, the dissolution rate varies at a given carbonate ion undersaturation ($\Delta[CO_3^{2-}]$). The effect on the reconstructed PETM deep-sea $[CO_3^{2-}]$ ion gradient between ocean basins is shown in Figure 10.

order mechanism. For example, the Caribbean and Walvis Ridge sites in the Atlantic are thousands of kilometers apart, yet the records from both sites are consistent with strong undersaturation. In the Pacific, given the locations of the Shatsky Rise and equatorial Pacific sites it is unlikely that the response of sediment production would have been uniform. Yet our reconstruction calls for less undersaturation at both locations. Thus the bottom water CO_3^{2-}-assumption provides a direct link between the observed dissolution pattern in each ocean basin. Any alternative hypothesis would have to offer an equally plausible explanation, one that accounts for the sequence of decreasing dissolution effects on Atlantic, Southern Ocean, and Pacific deep-sea sediments.

5. Model Sensitivity

[29] The simulations presented above require several assumptions regarding model parameter values. In order to test the robustness of the model results, we assessed the sensitivity of the model to variations in parameters such as dissolution strength, bioturbation, sedimentation rate, and clay flux.

5.1. Dissolution Parameter

[30] The standard model results were obtained using dissolution parameters $K = 5 \times 10^{10}$ mol m^{-2} y^{-1} and $\eta = 2.35$, similar to values employed in previous studies for the modern ocean [*Sigman et al.*, 1998] (see Appendix A for units and formula). For a bottom water undersaturation ($\Delta[CO_3^{2-}] = [CO_3^{2-}] - [CO_3^{2-}]_{sat}$) of -10 μmol kg^{-1}, the

dissolution rate is about 8 μmol cm^{-2} y^{-1}, comparable to measured dissolution fluxes in the modern deep ocean [e.g., *Martin and Sayles*, 1996]. However, given higher deep-sea temperatures during the PETM, it is possible that dissolution rates were higher. Standard parameters were set to produce dissolution rates tending towards the upper end of observations, particularly at stronger undersaturation. For this study, we neglect potential effects of variations in Eocene seawater composition and processes such as organic carbon respiration on dissolution which may have modified rates locally.

[31] We tested the sensitivity of the reconstructed deep-sea $[CO_3^{2-}]_{min}$ to variations in the dissolution parameters K and η (Figure 11). The results are shown in Figure 10. As expected, the dissolution strength affects the reconstructed basin gradient. For example, if the model's dissolution response to undersaturation is weak, the difference between $[CO_3^{2-}]_{min}$ of the basin end-members must be larger to produce the observed range of dissolution and vice versa. As a result, if the model's dissolution strength during the PETM, relative to the modern, would have to be assumed weaker, then the reconstructed PETM $[CO_3^{2-}]$ basin gradient is larger, see dashed line in Figure 10 (dotted line indicates the reverse case). However, potential variations in dissolution parameters does not affect our conclusion of a reversed $[CO_3^{2-}]$ basin gradient.

5.2. Bioturbation

[32] The bioturbation (mixing) depth in the standard model is $h_s = 10$ cm. This number defines the thickness of the top sediment layer and hence also the amount of
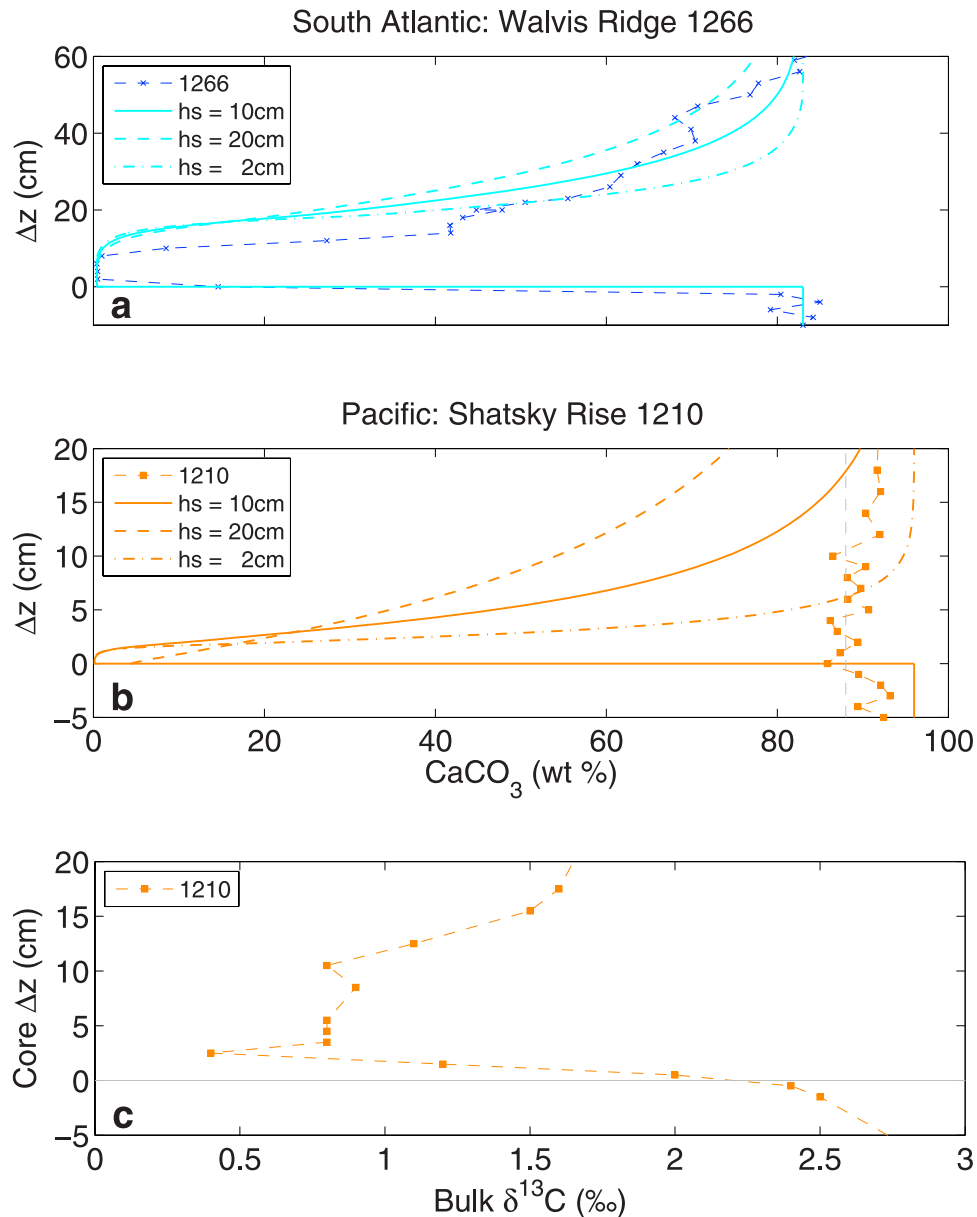
Figure 12. Effect of varying bioturbation depth, h_s, on the simulated temporal evolution of %CaCO$_3$ for (a) Atlantic Site 1266 at Walvis Ridge and (b) Pacific Site 1210 at Shatsky Rise. Irrespective of the value picked for h_s in the model, the essential features of the observations can be reproduced at Site 1266. This is not the case at Site 1210, including the smallest bioturbation depth of 2 cm. (c) Stable carbon isotope record (δ^{13}C) of bulk carbonate across the PEB at Site 1210 [*Colosimo et al.*, 2005], showing a sharp transition at the PEB. If remixing with old, previously deposited CaCO$_3$ had occurred, this feature would not have been preserved.

available CaCO$_3$ during erosion. In addition, the value of h_s influences the pace at which %CaCO$_3$ returns to initial values during the recovery phase. For example, a thin sediment mixed layer that transitions to clay during peak dissolution, can be filled with CaCO$_3$ more quickly than a thick mixed layer. However, h_s has no effect on the value of minimum %CaCO$_3$ during peak dissolution (feature 1, see section 4.1), provided that a quasi steady-state is established during maximum undersaturation, that is before the prescribed

deep-sea [CO$_3^{2-}$] starts to increase (see Figure 5). This holds for all "adjusted forcing" simulations (Table 1) except for Site 690 and the Shatsky Rise records. Varying h_s between 2 and 20 cm for these sites required [CO$_3^{2-}$]$_{min}$ to be adjusted by less than ± 3 μmol kg^{-1} in all cases in order to mimic observations (relative to the standard at $h_s = 10$ cm). Thus the effect of the bioturbation depth on the simulated [CO$_3^{2-}$] basin gradient is small.

[33] As mentioned above, bioturbation does affect erosion and the return to initial values. As an example, Figure 12 shows the effect of varying h_s between 2 and 20 cm on the temporal evolution of %CaCO$_3$ for Atlantic Site 1266 and Pacific Site 1210, which share similar paleowater depths (~2600 m). The essential features of the observations can roughly be reproduced at Site 1266, irrespective of the value picked for h_s. It appears that less (respectively more) vigorous bioturbation during the initial (later) stage of the recovery phase would yield a better fit to observations.

[34] Given the same forcing, the essential features at Site 1210 cannot be reproduced with the model, regardless of the value of h_s. Figure 12b also shows that the thickness of the low %CaCO$_3$ layer shrinks with smaller mixing depth. One explanation for the lack of thick clay layers at Shatsky Rise is that bioturbation only ceased during peak dissolution and resumed vigorously afterward, which could have mixed previously deposited CaCO$_3$ from below the excursion base into the surface. Such a homogenization with older carbonate could potentially lead to the disappearance of a thin clay layer. However, the single shell foraminifer δ^{13}C record across the PEB suggests the mixed layer is relatively thin at Site 1209, perhaps only 3–5 cm [Zachos et al., 2003]. Furthermore, bulk δ^{13}C values at Site 1210 decrease by ~2‰ over a distance of only 3 cm (Figure 12c). If substantial remixing with older sediment had occurred, the sharp transition would not have been preserved. This is also evident from the core photographs and holds for all Shatsky Rise records 1209–1212 [Colosimo et al., 2005].

[35] In summary, the assumption that the PETM dissolution pattern in the different ocean basins were caused by spatial differences in deep-sea [CO$_3^{2-}$] appears reasonable. Our reconstruction shows that bottom water in the Atlantic was more corrosive than in the Pacific. An alternative hypothesis that Atlantic and Pacific undersaturation was similar, appears unlikely. In particular, the absence of a clay layer in the Pacific Shatsky Rise records is difficult to reconcile. The sensitivity study indicates that the calculated deep [CO$_3^{2-}$] basin gradient is affected by the choice of dissolution parameters, much less so by bioturbation. The conclusion of a reversed PETM basin gradient relative to the modern is not compromised by either parameter and therefore appears a robust model result.

5.3. Age Models and Sedimentation Rates

[36] The age models for the various sites as derived by different investigators (cf. sections 4.1–4.5) are based on biostratigraphy and correlation of carbon isotope tie points to the record of Site 690 which has an astronomical age model. This may introduce errors of order 10^4 y in the age models used in the observational studies. However, this has little consequence for the simulation of the dissolution events in the current model. First, the CaCO$_3$ model-data comparison (Figures 4–9) is carried out in the depth domain with the assumption of constant fluxes through the excursion. We assume that the dissolution is driven by a global forcing that affects each ocean basin within a few thousand years. (We note that there is strong observational support that the event was global; even if the mixing time of the

ocean slowed, delays of of timescale $>10^4$ y would be unlikely.)

[37] Because the initial sedimentation rates are based on the published age models (Table 1), we have tested the sensitivity to this parameter as well. For example, in order to reproduce observations at Site 690 using SA forcing, the initial (preexcursion) sedimentation rate (1.5 cm ky^{-1}) would need to be increased by a factor of 6. Although there are significant uncertainties in the sedimentation rate at 690 during the excursion, astronomical- and ^{3}He-based rates do not indicate 6 times higher values anywhere during this interval [Farley and Eltgroth, 2003].

5.4. Enhanced Weathering Fluxes

[38] A number of processes can lower sediment %CaCO$_3$, including dissolution, decreased flux of CaCO$_3$, or increased flux of other material (e.g., clay). Drops in %CaCO$_3$ across the PETM in neritic sections have been ascribed to elevated siliciclastic fluxes and enhanced erosion [e.g., Crouch et al., 2003]. Although there is strong, independent evidence for dissolution in deep-sea environments during the PETM (e.g., fragmentation), we have also tested whether model results and observations can be reconciled by changes in clay fluxes, due for example, to accelerated continental weathering [e.g., Ravizza et al., 2001; Kelly et al., 2005]. Figure 13 addresses this question and shows sediment %CaCO$_3$ as a function of the clay rain based on a simple sediment equation (Appendix B) that includes rain, dissolution and burial (the complete model shows a very similar behavior). The degree of undersaturation is indicated by ζ (normalized to CaCO$_3$ rain; dissolution is %CaCO$_3$ times undersaturation, i.e., $f_c \times \zeta$).

[39] As the results indicate, it is improbable that increases in clay fluxes contributed significantly to the larger %CaCO$_3$ decreases in the deep-sea locations studied here, for instance, at Walvis Ridge. Irrespective of undersaturation, %CaCO$_3$ reductions to below 10% would require clay fluxes rising to considerably more than five times the initial value (the figure shows values for an initial clay flux of 15% relative to CaCO$_3$). If no undersaturation occurred at all ($\zeta = 0$), a five-fold increase could account for a drop from 87 to 57% in carbonate content $[100/(100 + 15)$ versus $100/(100 + 5 \cdot 15)]$. For comparison, as an indicator of enhanced weathering, Ravizza et al. [2001] estimated a rise in the flux of continental Os by a factor of 1.2–1.3 during the PETM. More importantly, in the case of strong undersaturation (e.g., $\zeta = 10$), the sediment CaCO$_3$ content is low and insensitive to changes in the clay flux.

[40] The reason is that for given CaCO$_3$ rain and sediment %CaCO$_3$, a stronger undersaturation can only be balanced by a drop in clay flux to the top of the sediment layer which reduces the CaCO$_3$ burial at the bottom (Appendix B). However, as soon as the clay flux approaches zero and ζ exceeds the carbonate rain, the balance must be maintained by decreasing %CaCO$_3$ (increasing the clay fluxes would reduce %CaCO$_3$ as well). As a result, because of the low sensitivity of %CaCO$_3$ to clay fluxes at strong undersaturation, the %CaCO$_3$-decreases in Atlantic cores cannot be reconciled with increased clay flux. For example, for Site 999 and SA forcing (Figure 6), a clay flux increase by more
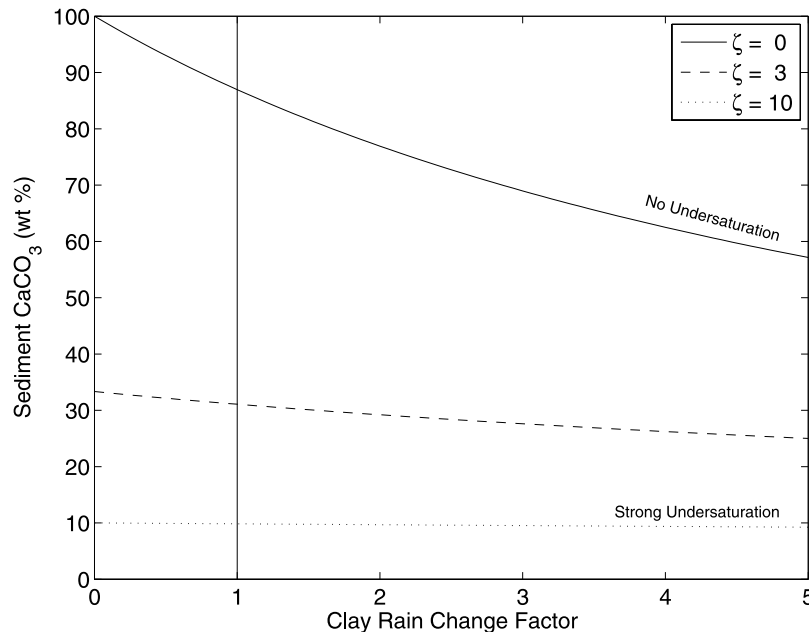
Figure 13. Sediment %$CaCO_3$ as a function of clay rain based on equation (B2). Initial clay rain is 15% of $CaCO_3$ rain (vertical line). Undersaturation is indicated by ζ (normalized to $CaCO_3$ rain). Note that sediment %$CaCO_3$ is insensitive to the clay flux for strong undersaturation.

than a factor of 50 would be required to approach observations. In fact, for Site 690 (Figure 7) a clay flux decrease (or carbonate rain increase) would actually be required because model %$CaCO_3$ is lower than observed. The former is opposite to the expected increase in continental weathering [*Ravizza et al.*, 2001; *Kelly et al.*, 2005].

[41] In summary, increases in clay fluxes are not a viable explanation for observed %$CaCO_3$ reductions in deep-sea sections, nor can they account for the discrepancy between model predictions and observations if a uniform undersaturation is applied. Similarly, changes in carbonate rain rate cannot be called on to explain our results. For example, to match data and model output for SA forcing at Sites 690 and 1210, 4.5, and 23 times higher $CaCO_3$ rain would be required, respectively.

6. Discussion

[42] Our results suggest that deep-sea [CO_3^{2-}] during the PETM dissolution interval increased from the Atlantic through the Southern Ocean into the Pacific. This pattern is reversed relative to the modern situation. In today's ocean, the distribution of [CO_3^{2-}] in the deep sea is mostly a result of deep water circulation and vertical fluxes of carbon and alkalinity due to the biological pump. Briefly, the "youngest" and least corrosive water, which was most recently in contact with the atmosphere, resides in the Atlantic. The "oldest" and most corrosive water, which has slowly accumulated respired CO_2, resides in the Pacific. In the late Paleocene prior to the onset of the PETM, it appears that circulation patterns were different than modern, with most deep-water formation in the Southern Ocean, and CCD levels roughly uniform, though slightly deeper in the

Atlantic. This balance was clearly perturbed during the PETM, but why?

[43] We stress that a sound hypothesis explaining our [CO_3^{2-}] reconstruction will require detailed modeling of physical and biogeochemical changes across the P/E boundary, which is beyond the scope of this paper. Nevertheless, one may speculate whether factors such as location of carbon input or ocean circulation, for instance, may have contributed to the reversed gradient. On the basis of a modern box model configuration, *Dickens* [2000] showed that oxidation of methane in the deep Atlantic would lead to more pronounced lysocline shoaling in the Atlantic compared to the Pacific. As a result, if the location of an oceanic carbon source was the primary reason for the reversed gradient as reconstructed here, carbon input into the deep Atlantic would be consistent with our findings. Note that reconstructing deep-sea [CO_3^{2-}] prior to the onset of the PETM or during the recovery phase is difficult with the current approach. Undersaturation, i.e., $\Omega \propto$ [CO_3^{2-}]/ [CO_3^{2-}]$_{sat} < 1$ is critical because sediment %$CaCO_3$ is sensitive to [CO_3^{2-}] for $\Omega < 1$, not for $\Omega > 1$.

[44] *Bice and Marotzke* [2002] examined the response of an Ocean General Circulation Model (OGCM with Eocene topography) to a gradual increase in the intensity of the atmospheric hydrologic cycle. The model showed an abrupt switch in deep water formation from dominant Southern Hemisphere sinking to Northern Hemisphere (Pacific) sinking (cf. however, *Thomas et al.* [2003]). As described above, the direction of today's ocean conveyor contributes to the modern deep-sea [CO_3^{2-}] gradient between Atlantic and Pacific. Everything else being equal, a reversed flow pattern should therefore result in a reversed gradient. Thus if a change in deep ocean circulation was the primary reason for

the reversed gradient, then a transient Pacific deep water source would be consistent with our results.

[45] This result conflicts with findings of *Nunes and Norris* [2006] who interpret an apparent reversal in benthic $\delta^{13}C$ gradients between sites in the northern Atlantic, Southern Ocean, and Pacific during the carbon isotope excursion (CIE) as evidence for Northern Hemisphere deep-water formation during the PETM, with the northern Atlantic as a possible source. We suspect that the reconstructed gradient reversal is actually a stratigraphic artifact created by the effects of dissolution on sediment accumulation in their northern Atlantic sites. Severe dissolution during the initial phases of the CIE would truncate the CIE as recorded by carbonates, including benthic foraminifera, biasing those records toward higher $\delta^{13}C$. If chemically eroded sediments or changes in accumulation rates are not accounted for, this would introduce error on the order of 10^4 y in the site-to-site correlations. If mean global $\delta^{13}C$ were constant, such error might be inconsequential. However, during times where $\delta^{13}C$ is rapidly changing, such as the CIE, even minor correlation errors could artificially create spatial gradients, where none actually existed.

7. Summary and Conclusion

[46] With our sediment model, we find that undersaturation with a globally homogenous deep-sea carbonate ion concentration during the PETM peak dissolution interval is inconsistent with constraints from deep-sea cores. Rather, the deep Atlantic carbonate ion content (degree of undersaturation) appears to have been significantly lower relative to the Southern Ocean and Pacific. The major implication of our reconstruction of PETM deep-sea $[CO_3^{2-}]$ is that the basin gradient was reversed relative to the modern. Uncertainties in model parameters related to local sediment fluxes do not appear to alter this finding. Still, some uncertainties remain, particularly regarding absolute concentrations. Likely causes for uncertainty include differences between modern and Eocene seawater composition/dissolution strength and potential variations in bioturbation (see section 5).

[47] Finally, it is emphasized that that identifying the cause of a reversed deep-sea carbonate ion basin gradient during the PETM will require thorough modeling of physical and biogeochemical changes across the Paleocene/Eocene boundary. This constitutes a significant challenge because the model results need to be verified with a suite of data, similar to but more detailed than available for the present study.

Appendix A: Sediment Model Equations

[48] Calcite and clay (rain, solid density $\rho = 2.5$ g cm^{-3}) are added to the bioturbated (well-mixed) top sediment layer of standard thickness $h_s = 10$ cm. Dissolution of calcite reduces the calcite content; net accumulation is hence rain minus dissolution. At the bottom of this layer, an amount equal to net accumulation is removed (via burial). If dissolution of CaCO$_3$ exceeds the rain of CaCO$_3$ plus clay, chemical erosion occurs. The sediment model equations thus include rain, dissolution, burial, and erosion. At variable porosity, the top layer can be separated into pure calcite plus pore water at porosity ϕ_1 (volume $A\ h_1$) and pure clay plus pore water at porosity ϕ_0 (volume $A\ h_2$). For variable porosity, the model equations can be conveniently written in terms of dh_1/dt. Conversion to df_c/dt merely requires multiplication by a factor. No attempt was made to include effects of organic carbon respiration on dissolution. However, dissolution parameters were varied over a wide range (Figures 10 and 11) to evaluate the sensitivity of model results to this effect.

[49] In the case in which rain exceeds dissolution, no erosion needs to be considered and we can write:

$$\frac{dh_1}{dt} = r_s^c - r_d - w^c \qquad (A1)$$

where r_s^c is the calcite rain rate, r_d is the calcite dissolution rate, and w^c is the calcite burial rate; all rates refer to volume of calcite plus pore water at porosity ϕ_1 per unit area and time (unit m y^{-1}). Total rates of calcite + clay + pore water are denoted by r_s and w. Burial = rain − dissolution, i.e., $w = r_s - r_d$, and the condition for no erosion is $w > 0$. Calcite and clay rain rate, r_s^c and r_s^r, are given by the input data for sedimentation rate and initial %CaCO$_3$ (Table 1); $r_s = r_s^c + r_s^r$. The dissolution rate, r_d, is calculated as

$$r_d = R_d\ k^0/\rho\ (1 - \phi_1) \qquad (A2)$$

$$R_d = f_c^{0.5}\ K\left(\left[CO_3^{2-}\right]_{sat} - \left[CO_3^{2-}\right]\right)^{\eta}/c^0. \qquad (A3)$$

where R_d is in mol m^{-2} y^{-1}, $k^0 = 100/10^3$ kg mol^{-1} converts from mol C to kg CaCO$_3$, and $c^0 = $ (mol kg^{-1})$^{\eta}$. In the standard model, $K = 5.0 \times 10^{10}$ mol m^{-2} y^{-1} and $\eta = 2.35$ [cf. *Sigman et al.*, 1998]. Note that η relates bottom water undersaturation to dissolution rate and is not to be confused with the calcite reaction order n, which relates pore water undersaturation to dissolution rate (typically $n = 4.5$). Finally, an expression is needed for the calcite burial, w^c, as a function of total burial w. The thickness of the pure calcite layer in Δz (= $w\ \Delta t$) can be expressed as $f_c\ \Delta z\ (1 - \phi)$ but also as $1 \cdot \Delta h_1\ (1 - \phi_1)$ (calcite fraction = 1), which gives

$$\Delta h_1 = f_c\ \Delta z\ \frac{1 - \phi}{1 - \phi_1} \qquad (A4)$$

or per unit time (rate):

$$w^c = f_c\ w\ \frac{1 - \phi}{1 - \phi_1}. \qquad (A5)$$

Inserting all the above expressions into equation (A1), the model equations can be solved. Because we took care of all individual porosities, the relationship between ϕ and f_c,

equation (3), is obeyed automatically (ϕ_0 and ϕ_1 are the porosities of a pure clay and calcite layer).

[50] In case of erosion ($w < 0$), it can be shown that

$$\frac{dh_1}{dt} = -(1 - f_c^0)\ (-w)\ \frac{1 - \phi^i}{1 - \phi_0} - r_s^r \qquad (A6)$$

where r_s^r is the clay rain rate (see above) and ϕ^i is the initial porosity. The total dissolution of pure calcite can be derived as

$$\frac{dh_c^d}{dt} = [(-w) + r_s]\ (1 - \phi_1). \qquad (A7)$$

Dissolution (removal) rate of calcite + pore water during erosion is $[(-w) + r_s]$. In other words, all calcite in Δz and rain is dissolved. In addition, calcite is replaced by the clay in Δz and by the clay rain (equivalent calcite is also dissolved). The model can also be formulated in terms of f_c:

$$\frac{df_c}{dt} = \frac{dh_1}{dt}\ G^{-1} \qquad (A8)$$

where

$$G = \frac{h_s}{1 - \phi_1} \left[(1 - \phi) - f_c \frac{\partial \phi}{\partial f_c} \right] \qquad (A9)$$

and

$$\frac{\partial \phi}{\partial f_c} = \frac{F\ (1 - \phi_0)}{(1 + f_c\ F)^2} \qquad (A10)$$

with $F = (\phi_1 - \phi_0)/(1 - \phi_1)$.

Appendix B: Effect of Clay Rain on %CaCO$_3$

[51] During steady state or if a quasi-steady state is maintained during peak undersaturation (which is the case in most simulations), we can write:

$$0 = \text{rain} - \text{diss.} - \text{burial} = r_s^c - r_d - w^c \qquad (B1)$$

or using expressions from Appendix A, assuming $\phi = const.$ and dissolution proportional to f_c:

$$0 = r_s^c - f_c\ \zeta - f_c\ (r_s^c + r_s^r - f_c\ \zeta) \qquad (B2)$$

where ζ measures the degree of undersaturation. Equation (B2) is a quadratic equation in f_c; values of the solution for f_c as a function of the clay rain (r_s^r) are shown in Figure 13. The behavior for $r_s^r \to \infty$ and $r_s^r \to 0$ is of importance. If the clay rain is large, the dominant burial term is $-f_c\ r_s^r$ and the solution for f_c reads:

$$f_c = \frac{r_s^c}{r_s^r + \zeta} \qquad (B3)$$

which shows that as $r_s^r \to \infty$, the decrease in f_c is inversely proportional to the clay flux. As the clay flux approaches zero, equation (B2) can be simplified to $0 = (f_c\ \zeta/r_s^c - 1)\ (f_c - 1)$, where ζ/r_s^c is the ratio of undersaturation to CaCO$_3$ rain. The relevant solution is

$$f_c = \frac{r_s^c}{\zeta} \qquad (B4)$$

which shows that for $r_s^r \to 0$, f_c is inversely proportional to the undersaturation.

[52] This demonstrates that during strong undersaturation, the sediment CaCO$_3$ content is insensitive to changes in the clay flux. If the clay flux is large and undersaturation strong, %CaCO$_3$ is low (equation (B3)). On the other hand, if the clay flux is small and undersaturation strong, %CaCO$_3$ is also low (equation (B4)). This is illustrated in Figure 13 for $\zeta = 10$. The complete numerical model shows a very similar behavior.

References

Archer, D. E. (1996), An atlas of the distribution of calcium carbonate in sediments of the deep sea, *Global Biogeochem. Cycles*, 10(1), 159–174.

Bice, K. L., and J. Marotzke (2002), Could changing ocean circulation have destabilized methane hydrate at the Paleocene/Eocene boundary?, *Paleoceanography*, 17(2), 1018, doi:10.1029/2001PA000678.

Bowen, G. J., et al. (2006), Eocene hyperthermal event offers insight into greenhouse warming, *Eos Trans. AGU*, 87, 165–169.

Bralower, T. J., D. J. Thomas, J. C. Zachos, M. M. Hirschmann, U. Röhl, H. Sigurdsson, E. Thomas, and D. L. Whitney (1997), High-resolution records of the late Paleocene thermal maximum and circum-Caribbean volcanism: Is there a causal link?, *Geology*, 25, 963–966.

Bralower, T. J., I. Premoli-Silva, and M. J. Malone (2002), Leg 198 summary, *Proc. ODP Init. Rep.*, 198, 1–148.

Bralower, T. J., D. C. Kelly, and D. J. Thomas (2004), Comment on "Coccolith Sr/Ca records of productivity during the Paleocene-Eocene thermal maximum from the Weddell Sea" by Heather M. Stoll and Santo Bains, *Paleoceanography*, 19, PA1014, doi:10.1029/2003PA000953.

Broecker, W. S., and T. Takahashi (1977), Neutralization of fossil fuel CO$_2$ by marine calcium carbonate, in *The Fate of Fossil Fuel CO$_2$ in the Oceans*, edited by N. R. Anderson and A. Malahoff, pp. 213–241, Plenum, New York.

Caldeira, K., and M. E. Wickett (2003), Anthropogenic carbon and ocean pH, *Nature*, 425, 365.

Colosimo, A. B., T. J. Bralower, and J. C. Zachos (2005), Evidence for lysocline shoaling and methane hydrate dissociation at the Paleocene-Eocene thermal maximum on Shatsky Rise, in *Proceedings of the Ocean Drilling Program, Scientific Results*, vol. 198, edited by T. J. Bralower, I. Premoli Silva, and M. J. Malone, 36 pp., Texas A&M Univ., College Station, Tex.

Crouch, E. M., G. R. Dickens, H. Brinkhuis, M.-P. Aubry, C. J. Hollis, K. M. Rogers, and H. Visscher (2003), The *Apectodinium* acme and terrestrial discharge during the Paleocene-Eocene thermal maximum: New palynological, geochemical and calcareous nannoplankton observations at Tawanui, New Zealand, *Palaeogeogr. Palaeoclimatol. Palaeoecol.*, 194, 387–403.

deMenocal, P. B., W. F. Ruddiman, and E. M. Pokras (1993), Influences of high- and low-latitude processes on African climate: Pleistocene eolian records from equatorial Atlantic Ocean Drilling Program Site 663, *Paleoceanography*, 8(2), 209–242.

Dickens, G. R. (2000), Methane oxidation during the late Palaeocene thermal maximum, *Bull. Soc. Geol. France*, 171(1), 37–49.

Dickens, G. R., J. R. O'Neil, D. K. Rea, and R. M. Owen (1995), Dissociation of oceanic methane hydrate as a cause of the carbon isotope excursion at the end of the Paleocene, *Paleoceanography*, 10, 965–971.

Dickens, G. R., M. M. Castillo, and J. C. G. Walker (1997), A blast of gas in the latest Paleocene: Simulating first-order effects of massive dissociation of oceanic methane hydrate, *Geology*, 25, 259–262.

Farley, K. A., and S. F. Eltgroth (2003), An alternative age model for the Paleocene-Eocene thermal maximum using extraterrestrial ^{3}He, *Earth Planet Sci. Lett.*, 208, 135–148.

Hancock, H. J. L., and G. R. Dickens (2005), Carbonate dissolution episodes in Paleocene and Eocene sediment, Shatsky Rise, West-Central Pacific, in *Proceedings of Ocean Drilling Program Scientific Results*, vol. 198, edited by T. J. Bralower, I. Premoli-Silva, and M. J. Malone, pp. 198SR–116, Texas A&M Univ., College Station, Tex.

Herbert, T. D., and L. A. Mayer (1991), Long climatic time series from sediment physical property measurements, *J. Sediment. Petrol.*, 61(7), 1089–1108.

Higgins, J. A., and D. P. Schrag (2006), Beyond methane: Towards a theory for the Paleocene-Eocene thermal maximum, *Earth Planet. Sci. Lett.*, 245, 523–537.

Kaiho, K., K. Takeda, M. R. Petrizzo, and J. C. Zachos (2006), Anomalous shifts in tropical Pacific planktonic and benthic foraminiferal test size during the Paleocene-Eocene Thermal Maximum, *Palaeogeogr. Palaeoclimatol. Palaeoecol.*, 237(2)–(4), 456–464.

Keir, R. (1982), Dissolution of calcite in the deep sea: Theoretical predictions for the case of uniform size particles settling into a well-mixed sediment, *Am. J. Sci.*, 282, 193–236.

Kelly, D. C., J. C. Zachos, T. J. Bralower, and S. A. Schellenberg (2005), Enhanced terrestrial weathering/runoff and surface-ocean carbonate production during the recovery stages of the Paleocene-Eocene thermal maximum, *Paleoceanography*, 20, PA4023, doi:10.1029/2005PA001163.

Kennett, J. P., and L. D. Stott (1991), Abrupt deep-sea warming, palaeoceanographic changes and benthic extinctions at the end of the Palaeocene, *Nature*, 353, 225–229.

Key, R. M., A. Kozyr, C. L. Sabine, K. Lee, R. Wanninkhof, J. Bullister, R. A. Feely, F. Millero, C. Mordy, and T.-H. Peng (2004), A global ocean carbon climatology: Results from GLODAP, *Global Biogeochem. Cycles*, 18, GB4031, doi:10.1029/2004GB002247.

Kurtz, A., L. R. Kump, M. A. Arthur, J. C. Zachos, and A. Paytan (2003), Early Cenozoic decoupling

of the global carbon and sulfur cycles, *Paleoceanography*, 18(4), 1090, doi:10.1029/2003PA000908.

Lyle, M., P. A. Wilson, and T. R. Janecek (2002), Leg 199 summary, *Proc. ODP Init. Rep.*, 199, 1–87.

Martin, W. R., and F. L. Sayles (1996), CaCO$_3$ dissolution in sediments of the Ceara Rise, western equatorial Atlantic, *Geochim. Cosmochim. Acta*, 60(2), 243–263.

Mayer, L. A. (1991), Extraction of high-resolution carbonate data for palaeoclimate reconstruction, *Nature*, 352, 148–150.

Millero, F. J. (1995), Thermodynamics of the carbon dioxide system in the oceans, *Geochim. Cosmochim. Acta*, 59, 661–677.

Mucci, A. (1983), The solubility of calcite and aragonite in seawater at various salinities, temperatures, and one atmosphere total pressure, *Am. J. Sci.*, 283, 780–799.

Murphy, B., M. Lyle, and A. O. Lyle (2006), Biogenic Burial across the Paleocene/Eocene Boundary: Ocean Drilling Program Leg 199 Site 1221, in *Proceedings of Ocean Drilling Project Scientific Results*, edited by P. A. Wilson, M. Lyle, and J. V. Firth, pp. 1–12, Texas A&M Univ., College Station, Tex.

Nunes, F., and R. D. Norris (2006), Abrupt reversal in ocean overturning during the Palaeocene/Eocene warm period, *Nature*, 439, 60–63.

Ravizza, G., R. N. Norris, J. Blusztajn, and M.-P. Aubry (2001), An osmium isotope excursion associated with the late Paleocene thermal maximum: Evidence of intensified chemical weathering, *Paleoceanography*, 16, 155–163.

Röhl, U., and L. J. Abrams (2000), High-resolution, downhole, and nondestructive core measurements from Sites 999 and 1001 in the Caribbean Sea: Application to the Late Paleocene thermal maximum, in *Proceedings of Ocean Drilling Project Scientific Results*, vol. 165, edited by R. M. Leckie et al., pp. 191–203, Texas A&M Univ., College Station, Tex.

Röhl, U., T. J. Bralower, R. D. Norris, and G. Wefer (2000), New chronology for the late Paleocene thermal maximum and its environmental implications, *Geology*, 28, 927–930.

Sigman, D. M., D. C. McCorkle, and W. R. Martin (1998), The calcite lysocline as a constraint on glacial/interglacial low-latitude production changes, *Global Biogeochem. Cycles*, 12(3), 409–427.

Sigurdsson, H., R. M. Leckie, and G. D. Acton (1997), Geologic studies of the Caribbean Sea, *Proc. ODP Init. Rep.*, 165, 7–13.

Sluijs, A., et al. (2006), Subtropical Arctic Ocean temperatures during the Palaeocene/Eocene thermal maximum, *Nature*, 441, 610–613.

Stoll, H. M. (2004), Reply to comment by T. J. Bralower, D. C. Kelly, and D. J. Thomas on "Coccolith Sr/Ca records of productivity during the Paleocene-Eocene Thermal Maximum from the Weddell Sea," *Paleoceanography*, 19, PA1015, doi:10.1029/2003PA000971.

Sundquist, E. T. (1986), Geologic Analogs: Their value and limitations in carbon dioxide research, in *The Changing Carbon Cycle: A Global Analysis*, edited by J. R. Trabalka and D. E. Reichle, pp. 371–402, Springer-Verlag, New York.

Svensen, H., S. Planke, A. Malthe-Sorenssen, B. Jamtveit, R. Myklebust, T. R. Eidem, and

S. S. Rey (2004), Release of methane from a volcanic basin as a mechanism for initial Eocene global warming, *Nature*, 429, 542–545.

Thomas, D. J., T. J. Bralower, and J. C. Zachos (1999), New evidence for subtropical warming during the late Paleocene thermal maximum: Stable isotopes from Deep Sea Drilling Project Site 527, Walvis Ridge, *Paleoceanography*, 14, 561–570.

Thomas, D. J., J. C. Zachos, T. J. Bralower, E. Thomas, and S. Bohaty (2002), Warming the fuel for the fire: Evidence for the thermal dissociation of methane hydrate during the Paleocene-Eocene thermal maximum, *Geology*, 30, 1067–1070.

Thomas, D. J., T. J. Bralower, and C. E. Jones (2003), Neodymium isotopic reconstruction of late Paleocene-early Eocene thermohaline circulation, *Earth Planet Sci. Lett.*, 209, 309–322.

Thomas, E., and N. J. Shackleton (1996), The Paleocene-Eocene benthic foraminiferal extinction and stable isotope anomalies, *Geol. Soc. London Spec. Publ.*, 101, 401–441.

Tripati, A., and H. Elderfield (2005), Deep-sea temperature and circulation changes at the Paleocene-Eocene thermal maximum, *Science*, 308, 1894–1898.

Tyrrell, T., and R. E. Zeebe (2004), History of carbonate ion concentration over the last 100 million years, *Geochim. Cosmochim. Acta*, 68(17), 3521–3530.

Zachos, J. C., M. Pagani, L. Sloan, E. Thomas, and K. Billups (2001), Trends, rhythms, and aberrations in global climate 65 Ma to present, *Science*, 292, 686–693.

Zachos, J. C., M. W. Wara, S. Bohaty, M. L. Delaney, M. Rose-Petrizzo, A. Brill, T. J. Bralower, and I. Premoli-Silva (2003), A transient rise in tropical sea surface temperature during the Paleocene-Eocene thermal maximum, *Science*, 302, 1551–1554.

Zachos, J. C., U. Röhl, S. A. Schellenberg, A. Sluijs, D. A. Hodell, D. C. Kelly, E. Thomas, M. Nicolo, I. Raffi, L. J. Lourens, H. McCarren, and D. Kroon (2005), Rapid acidification of the acean during the Paleocene-Eocene Thermal Maximum, *Science*, 308, 1611–1615.

Zeebe, R. E., and D. A. Wolf-Gladrow (2001), *CO$_2$ in Seawater: Equilibrium, Kinetics, Isotopes*, Elsevier Oceanogr. Ser., 346 pp., Elsevier, New York.

Zeebe, R. E., and P. Westbroek (2003), A simple model for the CaCO$_3$ saturation state of the ocean: The "Strangelove", the "Neritan", and the "Cretan" Ocean, *Geochem. Geophys. Geosyst.*, 4(12), 1104, doi:10.1029/2003GC000538.

————————————

J. C. Zachos, Earth and Planetary Sciences Department, University of California, Santa Cruz, Santa Cruz, CA 95064, USA. (jzachos@emerald.ucsc.edu)

R. E. Zeebe, School of Ocean and Earth Science and Technology, Department of Oceanography, University of Hawaii at Manoa, 1000 Pope Road, MSB 504, Honolulu, HI 96822, USA. (zeebe@hawaii.edu)